

# Upscaling of Two-Phase Flow Processes in Porous Media

HARTMUT EICHEL, RAINER HELMIG, INSA NEUWEILER, and OLAF A. CIRPKA

*Universität Stuttgart, Institut für Wasserbau,  
Pfaffenwaldring 61, 70569 Stuttgart, Deutschland*

**Abstract.** Intrinsic heterogeneities influence the multi-phase flow behavior of a dense non-aqueous phase liquids (DNAPL) infiltrating into a natural soil. Typically, we cannot resolve the scale of these heterogeneities so that upscaling techniques are required. The choice of the appropriate upscaling method depends on the averaging scale, since the relative importance of capillary and gravity forces change with scale. We present an easy and quick upscaling approach for cases in which the flow on the length-scale of heterogeneities is dominated by capillary forces.

The approach is based on a percolation model and a single-phase flow-averaging method. We apply the upscaling approach to experimental data of a DNAPL infiltration into a sandbox with artificial sand lenses. The anisotropy of the structure results in anisotropic flow which is amplified by the non-linear behavior of multi-phase flow. The residual saturation depends on the direction of flow, and the anisotropy ratio of the effective permeability is a function of the DNAPL saturation. Furthermore, it appears necessary to regard the relative permeability–saturation relationship as a tensor property rather than a scalar. The overall flow behavior simulated by the upscaled model agrees well with simulations accounting for the distinct lenses and the experimental data.

**Keywords:** two-phase flow, upscaling, saturation dependent anisotropy, porous media, macroscopic residual saturation, anisotropic relative permeabilities

## 1. Motivation

Multi-phase flow and transport processes in porous media play an important role in the remediation of non-aqueous phase liquids (NAPL) in the subsurface. These flow processes are affected by heterogeneities on all scales. Spatial variability ranges from single pores to geological structures, thereby spanning length scales from  $\mu\text{m}$  to km (see Figure 1).

Although the term *pore scale* is unambiguous, all other terms describing scales like micro or macro scale are not necessarily consistently used. For example, the typical length scales considered in petroleum engineering differ significantly from those in environmental engineering. While oil fields extend over hundreds of meters to kilometers, the typical scales for environmental problems range from meters to tens of meters (see Figure 2).

Different forces are likely to dominate on different scales. While on smaller scales capillary effects are more pronounced, the gravity effects and the viscous effects become more important at larger scales. For an environmental engineer, therefore, both the capillary and the gravity forces may be important. The dom-



© 2004 Kluwer Academic Publishers. Printed in the Netherlands.

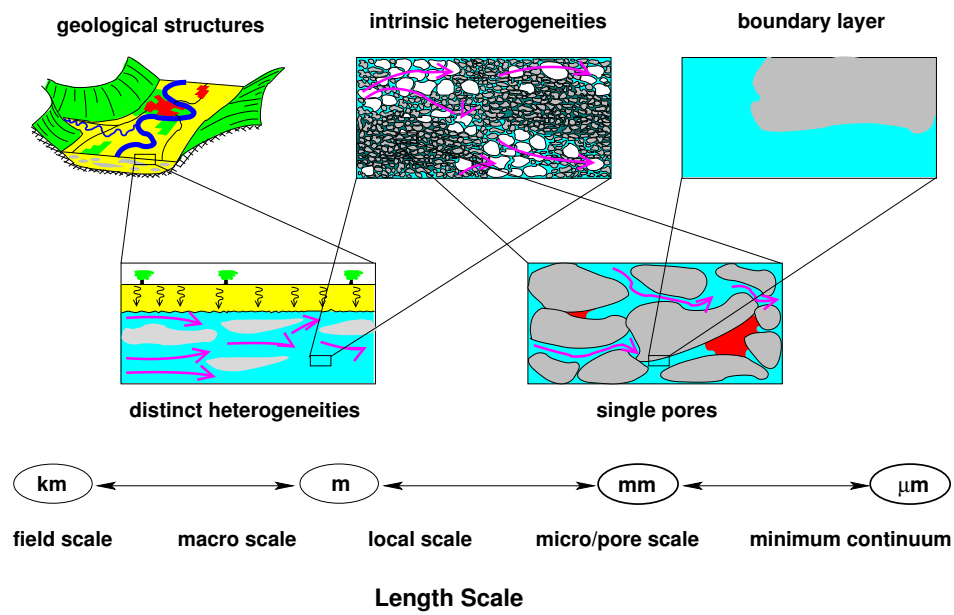


Figure 1. Scales in subsurface hydrology (after Kobus, de Haar, 1995)

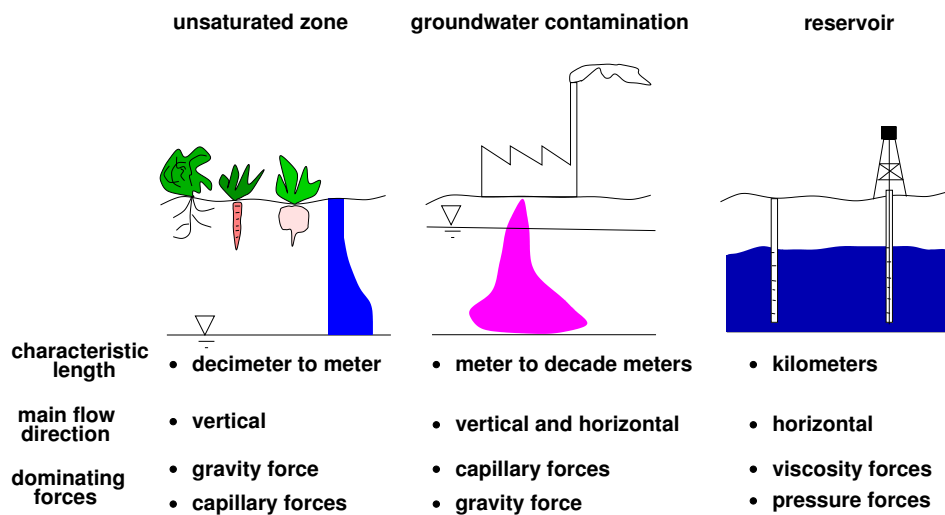


Figure 2. Different scales for different applications.

inating forces need to be determined prior to choosing a particular upscaling method.

In our example, we analyze an experiment carried out by (Allan et al., 1998; Kobus et al., 2000) at the research facility for subsurface remediation, VEGAS, at the University of Stuttgart. In the experiment, a dense non-aqueous phase liquid

(DNAPL) was infiltrated into a small sandbox. Figure 3 shows the distribution of sand types and the dimensions of the domain. The typical length scale is on the order of centimeters to decimeters, where gravity forces as well as capillary forces have to be considered.

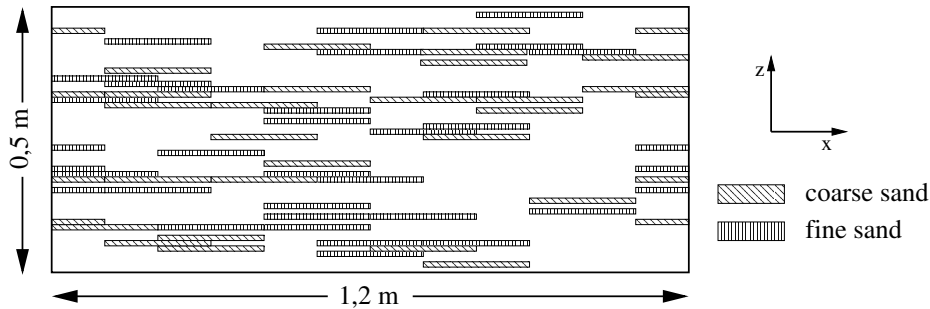


Figure 3. Distribution of the sand types in the experiment.

It is well known that small-scale structures, such as small-scale sand lenses, can influence multi-phase flow and transport significantly. Many laboratory experiments have shown that capillary forces have a large impact on the two-phase flow behaviour in porous media on almost all scales (Jakobs et al., 2003; Illangasekare et al., 1995).

This paper focuses on heterogeneities within larger-scale structures as seen in Figure 3. As is commonly known, the NAPL cannot penetrate a region of finer material as long as the capillary pressure has not yet exceeded the entry pressure. Thus, small-scale layering can lead to significant lateral spreading of the NAPL.

In spite of increasing computational power, the simulation of multi-phase flow in porous media is still restricted to comparably coarse grids, prohibiting the resolution of small-scale features. In the simulation of multi-phase flow on larger scales, it is therefore necessary to parameterize the effects of small-scale heterogeneities on the large-scale flow behavior. A variety of techniques have been developed and applied to transfer the information from the process scale to the simulation scale. These techniques are commonly referred to as upscaling. The upscaling techniques may be classified into the following categories:

- A-posteriori methods (effective parameters are derived from the analysis of highly resolved computation or measurement) [e.g. (Christie, 1996; Pickup and Sorbie, 1996; Dale et al., 1997; Chang and Mohanty, 1997)]
- Stochastic methods (determination of the effective parameters through assumptions of the statistical distribution of the heterogeneities and a stochastic averaging of the equations) [e.g. (Desbarats, 1995; Yeh et al., 1985; Man-

toglou and Gelhar, 1987; Chang et al., 1995; Neuweiler et al., 2003; Efendiev and Durlofsky, 2003)].

- Analytical methods (computation of the effective parameters for simple configurations, volume averaging) [e.g. (Quintard and Whitaker, 1988; Ahmadi and Quintard, 1996; Saez et al., 1989; Bourgeat and Panfilov, 1998)]
- Analogy methods (transformation of upscaling-approaches from other scopes of research to multi-phase flow) [e.g. (Wu and Pruess, 1986; Pruess, 1994; Pruess, 1996)]
- **Equilibrium methods** (simplification of the systems by assuming an equilibrium of forces) [e.g. (Corey and Rathjens, 1956; Smith, 1991; Ekrann et al., 1996; Yortsos et al., 1993; Kueper and Girgrah, 1994; Green et al., 1996; Pickup and Stephen, 2000; Braun et al., 2005)]. The focus here lies on the reduction of variables by assuming an equilibrium of (capillary) forces. This assumption allows for the application of a percolation model which, together with an appropriate averaging method, results in effective constitutive relationships for the macroscale.

The purpose of our upscaling approach is to compromise between two goals. First, we want to develop a relatively easy method, which is not restricted to a certain set of boundary and flow conditions and therefore applicable to different scenarios. Second, we want to reproduce the most important physical effects.

This paper is organized as follows. In Section 2, we present the experimental model set-up. We evaluate the validity of the capillary-equilibrium assumption by a dimensional analysis in Section 3. In Section 4, we introduce our upscaling approach. We compare the results of different models and the experiment in Section 5. In Section 6, finally, we draw conclusions and give an outlook to future studies.

## 2. Physical Model Setup

The physical experiment that we use as a reference was carried out by (Allan et al., 1998; Kobus et al., 2000).

### 2.1. PROPERTIES OF THE POROUS MEDIUM

A DNAPL is infiltrated into a water-saturated sandbox of dimensions ( $L \times W \times H$ )  $1.2 \text{ m} \times 0.08 \text{ m} \times 0.5 \text{ m}$ . The porous medium comprises three different sands, a fine, a medium, and a coarse one. The medium sand is the background material, while the other two are incorporated as lenses with a width of 0.2 m and a height of 0.01 m, see Figure 3. The properties of the sands are listed in Table 1. The medium sand occupies 80% of the domain whereas the fine and coarse sand take each 10%. The lenses are randomly distributed.

Table 1. Properties of the sands used in the experiment.

sand	fine	medium	coarse
permeability $k$ [m <sup>2</sup> ]	$6.38 \cdot 10^{-11}$	$1.22 \cdot 10^{-10}$	$2.55 \cdot 10^{-10}$
entry pressure $P_d$ [Pa]	882.9	539.55	353.16
form factor $\lambda$ [-]	3.0	3.0	3.2
residual saturation wetting phase $S_{wr}$ [-]	0.06	0.06	0.06
residual saturation non-wetting phase $S_{nr}$ [-]	0.10	0.15	0.10
porosity $\phi$ [-]	0.38	0.38	0.38
volume $w_i$ [%]	10	80	10

## 2.2. BOUNDARY AND INITIAL CONDITIONS

Initially, the entire domain is fully water-saturated, and there is no flow. This results in a hydrostatic pressure distribution. Over the entire course of the experiment, the left and the right faces of the domain are connected to a water reservoir ensuring constant pressure conditions at the boundaries. Water that is replaced by the infiltrating DNAPL can leave the system over these boundaries. The bottom and top boundaries are non-permeable for both liquids, except for a small stretch of two centimeters in the top, where the DNAPL infiltrates with a rate of  $0.4833 \cdot 10^{-6}$  m<sup>3</sup>/s for 2970 seconds. The initial and the boundary conditions are depicted in Figure 4.

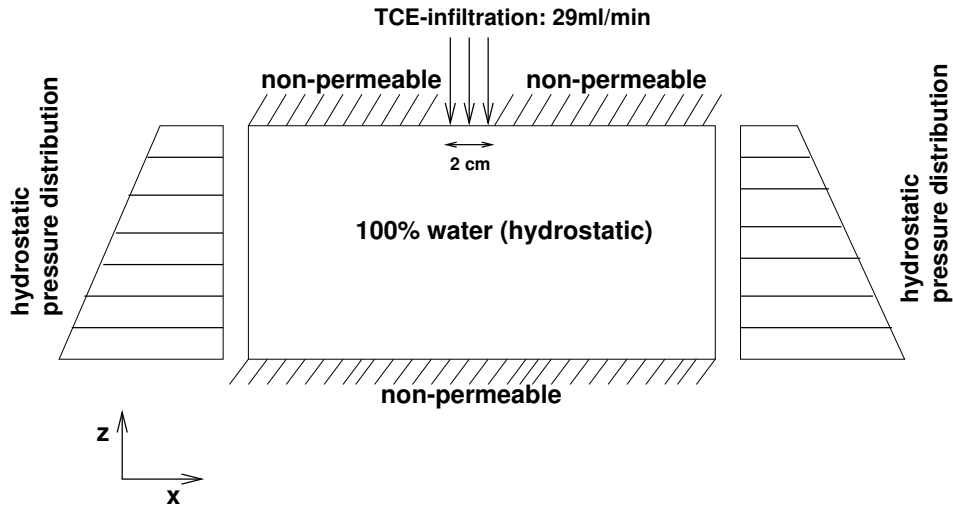


Figure 4. Initial and boundary conditions.

### 3. Mathematical Model and Dimensional Analysis

Our upscaling approach is based on capillary equilibrium. This means, that capillary forces are dominant on the small scale. In the following, we test this assumption by a dimensional analysis.

The system of the two-phase flow equations expresses the conservation of mass and generalized Darcy's Law of both fluids. We assume a rigid solid phase and incompressible fluids. The following equations describe the flow on the local scale.

$$\phi(\vec{x}) \frac{\partial S_w}{\partial t} + \vec{\nabla} \cdot \left( -\frac{k_{r,w}(S_w, \vec{x})}{\mu_w} k(\vec{x}) (\vec{\nabla}(P_w) + \varrho_w \vec{g}) \right) = q_w \quad (1)$$

$$\phi(\vec{x}) \frac{\partial S_n}{\partial t} + \vec{\nabla} \cdot \left( -\frac{k_{r,n}(S_n, \vec{x})}{\mu_n} k(\vec{x}) (\vec{\nabla}(P_n) + \varrho_n \vec{g}) \right) = q_n \quad (2)$$

where  $\phi$ ,  $\varrho$ ,  $S$ ,  $\mu$ ,  $g$ ,  $P$ , and  $q$  are the porosity, the density, the saturation, the viscosity, the acceleration constant due to gravity, the phase pressure and the source/sink term, respectively.  $k$  is the intrinsic permeability,  $k_r$  is the relative permeability of the respective phase, and  $k_{eff} = k_r k$  is the effective permeability. The subscripts  $n$  and  $w$  denote the non-wetting and the wetting phase. For a detailed derivation of this formulation see, e.g., (Marle, 1981; Helmig, 1997).

These two equations are coupled by the two following relations. First, the two saturations sum up to unity. Second, the capillary pressure, defined as the difference between the pressure of the non-wetting and the wetting fluids, is a unique function of the saturation.

$$S_n + S_w = 1, \quad P_c(S_n) = P_n - P_w. \quad (3)$$

In the dimensional analysis, we assume that the source/sink terms,  $q_w$  and  $q_n$ , are zero. We sum up the two equations and introduce the total Darcy velocity  $\vec{u}_{total} = \vec{u}_n + \vec{u}_w$ . In that way, we eliminate the phase pressures and the phase Darcy velocities from the equation. The two-phase continuity equation reads:

$$\phi \partial_t S_n + \vec{u}_{total} \cdot \vec{\nabla} f(S_n) + \vec{\nabla} \cdot \left( \frac{g k \Delta \rho}{\mu_n} \Lambda(S_n) \vec{e}_z \right) - \vec{\nabla} \cdot \left( \frac{k}{\mu_n} \Lambda(S_n) \vec{\nabla} P_c \right) = 0. \quad (4)$$

The fractional flow function  $f(S_n)$  of the non-wetting fluid is defined as:

$$f(S_n) = \frac{k_{r,n}(S_n)}{k_{r,n}(S_n) + \frac{\mu_n}{\mu_w} k_{r,w}(S_n)}, \quad (5)$$

and  $\Lambda(S)$  stands for

$$\Lambda(S_n) = \frac{\frac{\mu_n}{\mu_w} k_{r,n}(S_n) k_{r,w}(S_n)}{k_{r,n}(S_n) + \frac{\mu_n}{\mu_w} k_{r,w}(S_n)} = \frac{\mu_n}{\mu_w} k_{r,w} f(S_n). \quad (6)$$

The density difference is defined as  $\Delta\rho = \rho_n - \rho_w$ .

As a first approximation we assume that we can neglect horizontal total flow velocities due to pooling and have therefore only capillary forces acting in horizontal direction.

We introduce typical scales for time, length, and capillary pressure. The time is scaled with gravity. Typical length scales are the dimensions of the domain,  $X$  and  $Z$ , and the capillary pressure is scaled by the entry pressure  $P_d$ ,

$$t^\star = \frac{t k \Delta\rho g}{Z \mu_n}, \quad z^\star = z/Z, \quad x^\star = x/X, \quad P_c^\star = P_c/P_d \quad (7)$$

in which the star denotes dimensionless variables. Thus, we obtain the following dimensionless form of equation 4:

$$\partial_{t^\star} S_n + \mathbf{Gr}^{-1} \partial_{z^\star} f(S_n) + \partial_{z^\star} \Lambda(S_n) - \mathbf{Bo}_z^{-1} \partial_{z^\star} \Lambda(S_n) \partial_{z^\star} P_c^\star(S_n) - \mathbf{Bo}_x^{-1} \partial_{x^\star} \Lambda(S_n) \partial_{x^\star} P_c^\star(S_n) = 0 \quad (8)$$

with the inverse gravity number  $\mathbf{Gr}^{-1}$  and the inverse Bond numbers  $\mathbf{Bo}^{-1}$  in the  $x$  direction and in the  $z$  direction.

$$\mathbf{Gr}^{-1} := \frac{\text{viscous forces}}{\text{gravity forces}} = \frac{\mu \cdot u}{\Delta\rho \cdot g \cdot k} \quad (9)$$

$$\mathbf{Bo}_z^{-1} := \frac{\text{capillary forces}}{\text{gravity forces}} = \frac{P_d}{\Delta\rho \cdot g \cdot Z} \quad (10)$$

$$\mathbf{Bo}_x^{-1} := \frac{\text{capillary forces}}{\text{gravity forces}} = \frac{P_d \cdot Z}{\Delta\rho \cdot g \cdot X^2} \quad (11)$$

The capillary effects are accounted for by the Bond numbers. As an alternative, one may use the capillary number  $\mathbf{Ca}$ , which is related to the Bond number by:

$$\mathbf{Ca} = \frac{\text{capillary forces}}{\text{viscous forces}} = \frac{\mathbf{Gr}}{\mathbf{Bo}}. \quad (12)$$

We evaluate these quantities on the large (domain) scale. Considering the typical parameter values for the background sand material  $k = 1.22 \cdot 10^{-10} \text{ m}^2$ ,  $P_d = 540 \text{ Pa}$ , the length scales of the domain  $Z = 0.5 \text{ m}$ ,  $X = 1.2 \text{ m}$ , and the liquid properties  $\Delta\rho = 460 \text{ kg/m}^3$ ,  $\mu_n = 5.7 \cdot 10^{-4} \text{ kg/(ms)}$ , the only quantity that we have to evaluate is the characteristic velocity  $u$ . A rough estimation is given by assuming only the vertical component. The injected volumetric flux is  $Q = 4.8 \cdot 10^{-7} \text{ m}^3/\text{s}$ , the width of the inlet is 2 cm, and the box is 8 cm thick. This yields a maximum vertical darcy velocity of  $u_{\text{total}} = 3 \cdot 10^{-4} \text{ m/s}$ . We assume that the velocity of the wetting phase is negligible. If we insert these values into equations 9 – 11, we get the following values of the three characteristic

dimensionless numbers.

$$\mathbf{Gr}^{-1} = 0.31, \quad \mathbf{Bo}_z^{-1} = 0.24, \quad \mathbf{Bo}_x^{-1} = 0.04. \quad (13)$$

For the detailed flow process we have to consider the small length scale, given by the dimension of the inclusions. If we introduce the ratio between the length scales of the inclusions and the domain (Duijn et al., 2002),

$$\epsilon_{vert.} = \frac{\Delta z}{\Delta Z} = 0.02, \quad \epsilon_{horiz.} = \frac{\Delta x}{\Delta X} = 0.17, \quad (14)$$

the spatial derivatives on the small and large scales can be separated. Having chosen the base system to be the large (domain) scale, the spatial derivatives on the small scale are multiplied by a factor of  $1/\epsilon$ . Since the expressions accounting for “diffusive” processes have second-order spatial derivatives, they are scaled by  $1/\epsilon^2$  on the small scale, whereas the “advective” processes are scaled by  $1/\epsilon$  on the small scale. In this way, the capillary processes are “magnified” on the small scale, and their impact is higher than on the large scale. If the respective inverse Bond numbers are small (the same order as  $\epsilon$ ), the “magnification” of the capillary processes on the small scale cancels out and advective and diffusive processes contribute on the small scale to the same extent.

If the capillary number is of order 1 and large compared to  $\epsilon$ , the diffusive processes on the small scale are weighted by  $1/\epsilon$  compared to the advective processes. In this case, the small scale is dominated by capillary forces, and the viscous and gravity forces on this scale can be neglected.

In order to meet the criterion for capillary dominance, a clear separation of scales must be given:

$$\epsilon \ll \mathbf{Bo}^{-1} \ll 1/\epsilon \quad \epsilon \ll \mathbf{Ca}^{-1} \ll 1/\epsilon. \quad (15)$$

In our case, the separation criterion is met in the vertical direction,  $\epsilon = 0.02 < \mathbf{Bo}_z^{-1} = 0.24 \ll 1/\epsilon = 50$ . As the inverse gravity number is between 0.1 and 1, the criterion (15) is also met for the inverse capillary number.

Although the criterion for capillary equilibrium is met in the experiment considered here, the following points should be considered:

- The analysis holds only when the inclusions are placed in distances in the same range as the length scale of the inclusion. Otherwise we get the average distance of the inclusions as an additional intermediate scale. Also, the contrast of the parameter properties, such as permeability and capillary entry pressure has to be large compared to  $\epsilon$  and small compared to  $1/\epsilon$ . Obviously the difference of the function  $\Lambda(S_n)$  in the different materials should also not be large, in order to keep the scales separated.



- We could also use the small scale as the base system and scale all numbers accordingly with the small length scales. By this, we would obtain identical results.
- The actual experimental setup is more complex. The influx is not placed over the whole width of the tank. The estimation for the resulting vertical and horizontal total flow velocities is therefore not trivial.

## 4. Upscaling Method

In this section, we describe the different underlying assumptions and the steps comprising the proposed upscaling approach, used to derive effective parameters on the macroscale for the simulation of two-phase flow processes. This is done by a percolation model and a small-scale flow-averaging method.

### 4.1. ASSUMPTIONS

As outlined above, we assume that capillary effects dominate the processes on the small scale. Changes of variables on the large scale are very slow compared to changes of variables on the small scale. From the perspective of the large scale, this implies that the small-scale reaction on a change of large-scale variables is quasi instantaneously. Thus, we can neglect the dynamics on the small scale and assume, on that scale, that the system is in capillary equilibrium. We make use of that property in a percolation model for the small-scale features. Here, we assume that, given a large-scale capillary pressure, the non-wetting phase enters instantaneously all cells of the small-scale model in which the entry pressure is exceeded. Therefore hysteresis does not play a role in this model. The fluid distribution in the small-scale model is given from the local  $P_c - S$  relations that are represented by Brooks-Corey type functions (Brooks and Corey, 1966), with no residual saturation ( $S_{nr}$ ) on the local scale. By this means, we can construct the functional relation between the capillary pressure and the large-scale saturation.

### 4.2. PERCOLATION MODEL

In our application, we know the exact distribution of the materials with their parameters and constitutive relationships. Applying the capillary equilibrium assumption to a distribution of local  $P_c - S_w$  relationships, we can determine the saturation distribution for a given capillary pressure. We do this by applying a static site-percolation model (Stauffer, 1985). The arithmetic mean of the saturation distribution gives one point on the macroscopic capillary pressure-saturation-relationship. In Figure 5, three different capillary pressure levels and the associated macroscopic saturations are shown. The three resulting points on the macroscopic curve are shown in Figure 6.

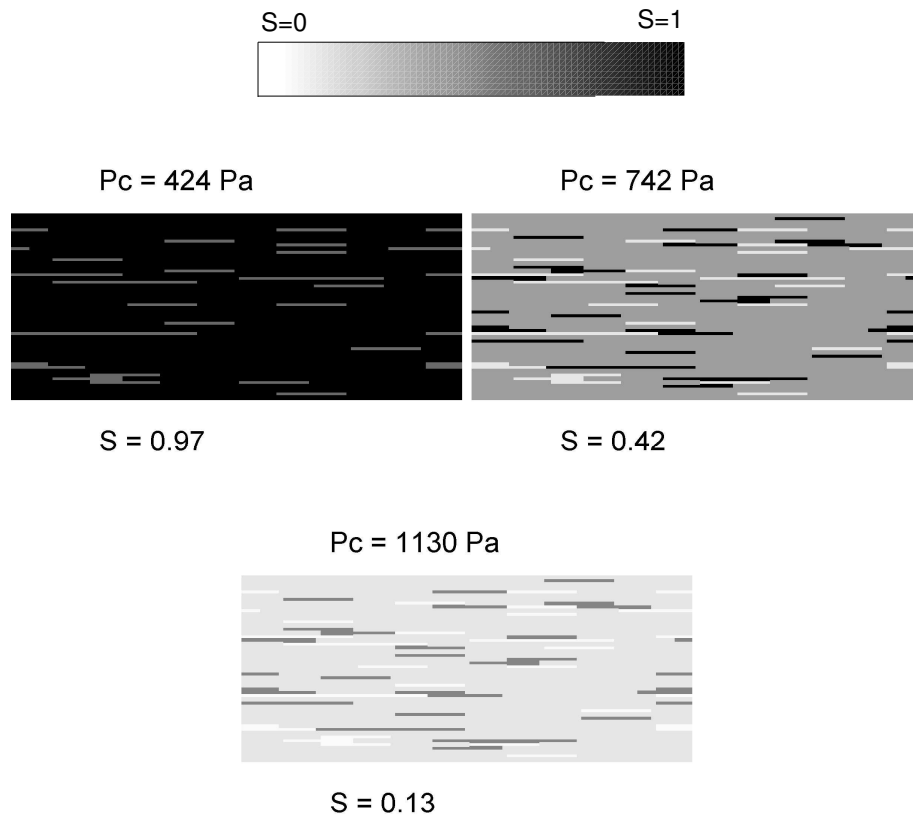


Figure 5. Steps in the percolation model.

Cycling through this procedure with different capillary pressures, one can determine the complete macroscopic capillary pressure–saturation relationship.

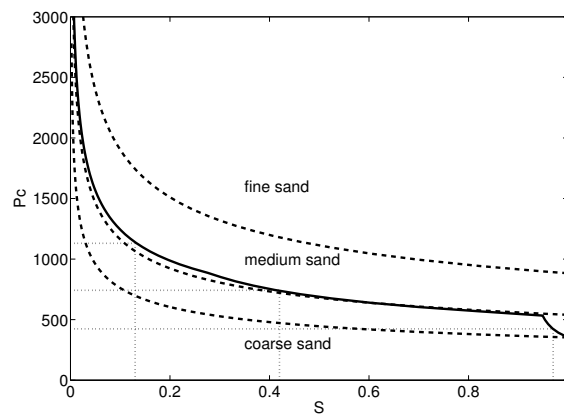


Figure 6. Macroscopic capillary pressure – saturation relationship

In Figure 6, four different  $P - c - S$  relationships are shown. The three dashed curves indicate the relationships for the three individual sands, while the solid line is the determined macroscopic  $P_c$ - $S$ -relationship. The  $P_c - S$  relationship resembles the curve of the medium sand quite closely (Figure 6). Only at high saturations of the wetting fluid, the upscaled curve shows a dip that does not exist in the retention curve of the medium sand. At this saturation the entry pressure of the background sand is exceeded.

#### 4.3. RENORMALIZATION

As a first upscaling approach for the relative permeabilities, we test the renormalization approach as suggested by Williams and King (Williams, 1989; King, 1996). For a quadratic domain the effective horizontal conductivity  $\overline{k_h}$  can be computed by a finite difference method. The indices are shown in Figure 7.

$$\overline{k_h} = \frac{2 \cdot (k_1 + k_2) \cdot (k_3 + k_4) \cdot (k_{12}^h + k_{34}^h)}{3 \cdot (k_1 + k_3) \cdot (k_2 + k_4) + \frac{1}{2} \cdot (k_1 + k_2 + k_3 + k_4) \cdot (k_{12}^h + k_{34}^h)}, \quad (16)$$

$$\text{with } k_{ij}^h = \frac{2 \cdot k_i \cdot k_j}{k_i + k_j}. \quad (17)$$

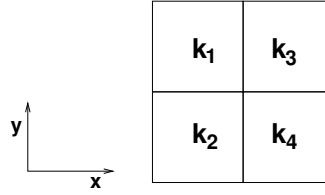


Figure 7. Indices used in the renormalization method.

For the effective vertical conductivity, the indices “2” and “3” have to be exchanged. After determining the effective conductivity of a block of four cells, one proceeds to a higher scale on which the conductivities of four blocks are averaged.

For every specific global saturation, there exists a local saturation distribution computed by the percolation model. The local  $k_{eff} = k_r(S)k$  is thus known. The renormalization is performed for the effective permeability. On the highest level, the procedure results in a single effective permeability for each phase in each direction. As the relative permeability  $kr$  is defined by

$$kr_{ii} = \frac{k_{eff,ii}(S)}{k_{eff,ii}(S=1)}, \quad \text{with } i = x, y, \quad (18)$$

the renormalization yields one point on the upscaled relative permeability - saturation relationship. Repeating this procedure with different capillary pressures,

and thus different saturations, yields the two upscaled  $kr_w - S_w$ -relationships. This procedure is carried out for both spatial dimensions and both fluids.

It may be noteworthy that the strong anisotropy on the small scale and the harmonic weighting in the renormalization procedure yields artefacts, as can be seen in Figure 8. Here, the dashed lines indicate Brooks-Corey parameterized curves (Brooks and Corey, 1966) used as parameterizations for all materials. The solid lines represent the vertical  $kr - S$ -relationships computed by the renormalization method. The horizontal  $kr - S$ -curves, which are not shown here, are closer to the Brooks-Corey parameterizations.

The renormalization method leads to extremely high macroscopic residual saturations caused by zones of relatively low permeabilities. This may be explained by the illustrative example shown in Figure 9. In this example, a preferential, curvilinear flow path exists. The unfortunate choice of the first renormalization blocks, however, cuts the preferential flow path off. Thus, effective permeability on the highest level is strongly underestimated.

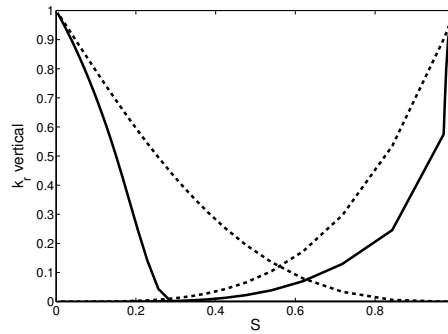


Figure 8.  $kr - S$  relationship obtained from the renormalization method.

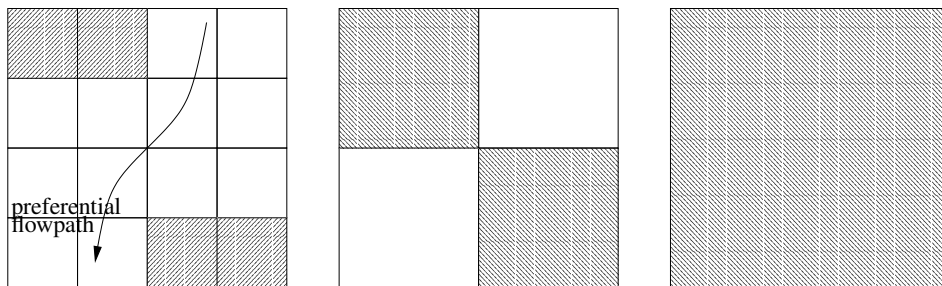


Figure 9. Renormalization techniques for anisotropic systems.

#### 4.4. SINGLE-PHASE FLOW-AVERAGING METHOD

The upscaled relative permeability - saturation relationship can be computed by solving the pressure equation for a single phase (Dykaar and Kitanidis, 1992). Periodic boundary conditions are chosen, so that the pressure fluctuations match on opposing sides. Imposing a large-scale pressure gradient onto the system, the pressure at the inflow boundary has a higher value than that at the outflow boundary. This is accounted for by a uniform jump. The general setup of periodic cells used for upscaling is well described by (Durlafsky, 1991).

Our procedure is as follows. For a given capillary pressure, the local saturation distribution is known from the percolation model. This together with the known local  $k_r$ - $S$  relationship and the permeability distribution, yields the local effective permeability. We now solve the pressure equation for a single phase, imposing a unit pressure gradient. It is assumed that the motion of one fluid has no impact on that of the other fluid. From the pressure distribution of the single fluid we can determine its velocity field. Then, the effective permeability of the phase considered,  $k_{eff}$ , can be calculated from the mean velocity and the applied pressure gradient.

Since the relative permeability is defined as the ratio between  $k_{eff}$  ( $S = 1$ ) and  $k_{eff}$  ( $S$ ), the single-phase flow simulation yields a single point on the upscaled relative permeability - saturation relationship. Repeating the analysis for different capillary pressures, and thus different saturations, we construct the entire relative permeability curve. The procedure is carried out for both fluids independently.

The effective permeability value obtained is one diagonal entry in the effective permeability tensor. In order to get the second diagonal entry, another set of flow simulations is carried out, now with the pressure gradient perpendicular to the first direction. Applying periodic boundary conditions without jump along the remaining boundaries, we also determine the off-diagonal entries of the relative-permeability tensor. In the present application, however, these terms are comparably small and are thus neglected in the following analysis.

Figure 10 shows the relative permeabilities for the above explained single-phase flow averaging method, applied to the data of the sandbox. The solid lines indicate the vertical relative permeabilities, the dashed lines represent the horizontal relative permeabilities, while the dotted lines show Brooks-Corey parametrizations for the medium sand as comparison. It is clearly visible that the vertical relative permeabilities are highly reduced compared to the local Brooks-Corey curves and that the horizontal ones are slightly increased. That is, the relative permeability exhibits strong anisotropy. Also, the macroscopic residual saturations differ from the residual saturation of the Brooks-Corey curve. Both findings are in agreement with the experimental results. The lenses lead to more horizontal spreading and delay the flow in the vertical direction. In the coarse sand lenses DNAPL gets trapped, while the fine sand lenses can be bypassed. Although the

macroscopic residual saturations for flow in the vertical direction increases, they are not as high as computed by the renormalization method.

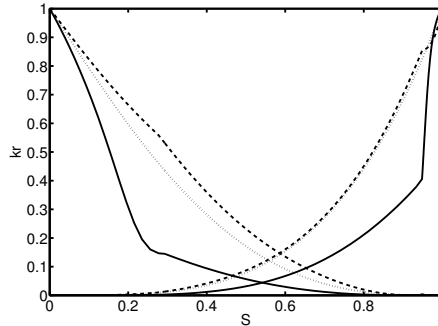


Figure 10.  $k_r$  -  $S$  relationships obtained from the single-phase simulations.

Applying periodic boundary conditions in the single-phase flow simulations implies that the domain with the small-scale features is interpreted as a unit cell of a periodic domain, made of an infinite number of those unit cells. By construction, the unit cell of such a system is a representative elementary volume. The periodic boundary conditions also guarantee that the resulting effective permeability tensor is symmetric and positive-definite. When the saturation of the considered phase becomes extremely small, however, numerical errors may cause prohibited effective-permeability tensors.

## 5. Comparison of Measured and Simulated NAPL Distributions

We now compare the experimental saturation distribution (see Figure 11) with a discrete, two-dimensional simulation (see Figure 12), in which the blocks of different permeability are resolved explicitly. We use a boxmethod as described in (Helmig, 1997) solving the discretized equations for water pressure and DNAPL saturation. The grid cells are 1 cm high and 2 cm wide. The experimental results are based on photographs taken after one hour. The exact saturation values cannot be determined, nonetheless, the picture gives a good qualitative impression of how far the NAPL distribution infiltrated.

The detailed simulation reproduces the experiment well with respect to the overall NAPL distribution. The experimental data are almost binary, with NAPL found in a few coarse-sand lenses. Here, the NAPL is entrapped by capillary forces. The simulations predict quite well which coarse-sand blocks are occupied by the NAPL. The simulations, however, show a higher residual saturation in the medium-sand matrix than observed in the experiment. On the macro-scale, the residual saturation is dominated by the entrapment in the coarse-sand lenses. In the simulations, we can also identify some fine-sand lenses by the non-wetting phase pooling on top of them. If we take two threshold values for the saturation, namely

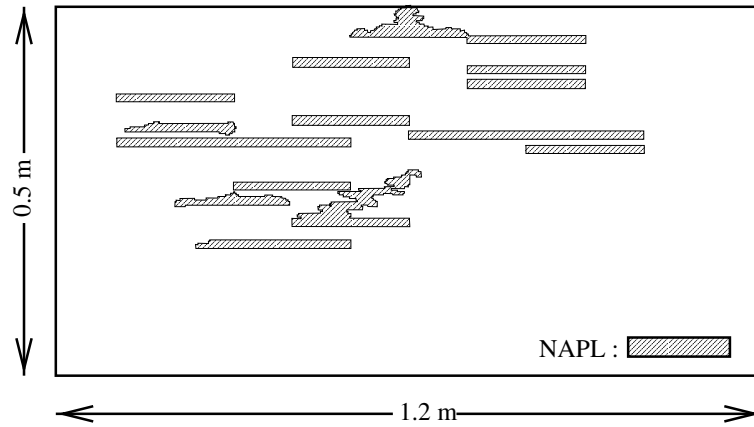


Figure 11. Experimental NAPL distribution after 1 hr (from Braun, 2000).

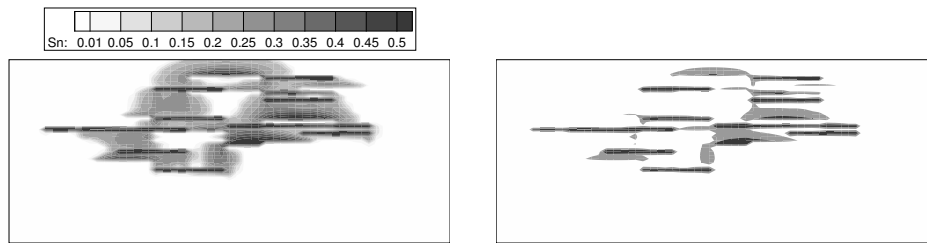


Figure 12. Discrete simulations. Left: full saturation distribution; right: two threshold values of 0.3 and 0.5.

0.3 and 0.5, we see how closely the numerical results match the experimental data.

After we have shown that the discrete simulation matches the experimental results well; we now compare these results with two simulations based on up-scaled constitutive relationships. This allows us to calculate and compare first and second moments of the DNAPL body, which would have not been possible with the experimental results.

The first is a simple upscaling approach, where the permeabilities and entry pressure are just geometrically averaged to obtain the macroscopic parameters. The absolute permeability should be anisotropic due to the different correlation lengths but the influence is negligible. The relative permeabilities are approximated as Brooks-Corey parametrizations. In Figure 13, we see that the macroscopic parameters obtained by taking the geometrical average of the small scale values, cannot capture the overall flow behaviour. In this example, the downward velocity is overestimated dramatically, and the horizontal spreading is not represented.

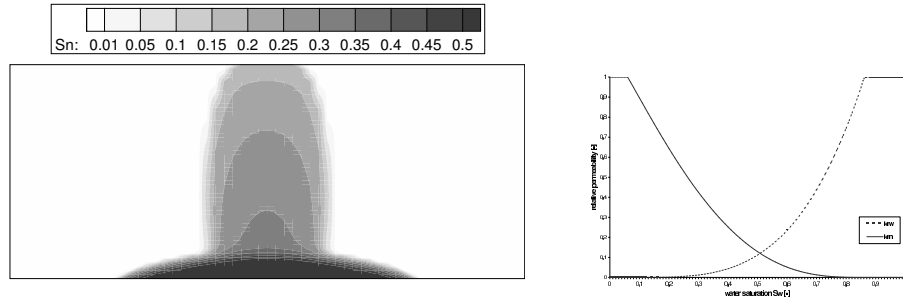


Figure 13. Saturation distribution for upscaling by taking the geometric average.

Figure 14 shows the results for two different grids using the upscaled constitutive relationships from the percolation model and the single-phase flow-approach for the relative permeabilities. The left simulation is computed on a grid which is as fine as the one used for the detailed simulations. The results shown in right sub-plot are obtained on a coarser grid. The predicted distributions are very similar.

For the simulations shown in Figure 14, we have upscaled the entire domain. That is, the system is considered homogeneous with identical parameters and constitutive relationships throughout the domain. Consequently, one cannot expect to see small-scale features of the saturation distribution. However, two overall trends are identical in the upscaled and detailed simulations as well as in the experiments. First, the vertical velocity of the DNAPL is retarded, and second, the horizontal spreading of the DNAPL is enhanced. The upscaled simulations reproduce those features because the vertical relative permeability curves (solid curves) seen in Figure 10 are well below the Brooks-Corey parametrizations indicated by the dotted lines, and the horizontal relative permeability curve, at least of the DNAPL, is larger. These curves reflect the effect of the lenses in the physical model that diminish downward movement of the DNAPL.

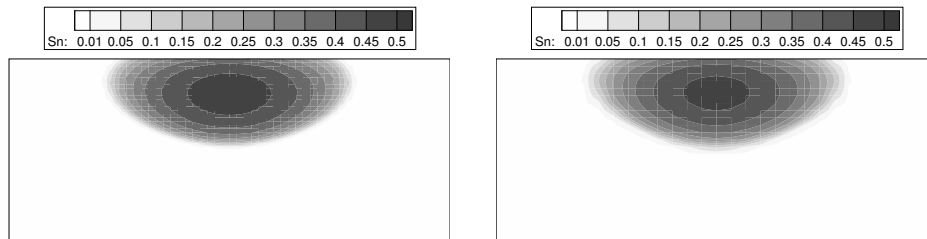


Figure 14. Saturation distribution for the upscaled anisotropic parameters – left: Fine grid simulation – right: Coarse (upscaled) grid simulation

In Figure 15, we overlay the numerical results of the discrete simulation with the proposed upscaling approach. The contour lines show the saturation distribution from the simulation with the upscaled values, while the gray and black areas indicate regions where the DNAPL exceeds a saturation of 0.3 and 0.5,



respectively.

On average, the lateral spreading is matched well. Obviously, coarse-sand lenses extending beyond the region, that is reached by the DNAPL in the upscaled simulation, cannot be captured fully. The vertical migration is slightly underestimated, indicating an overestimation of macroscopic residual saturation by the upscaling approach.

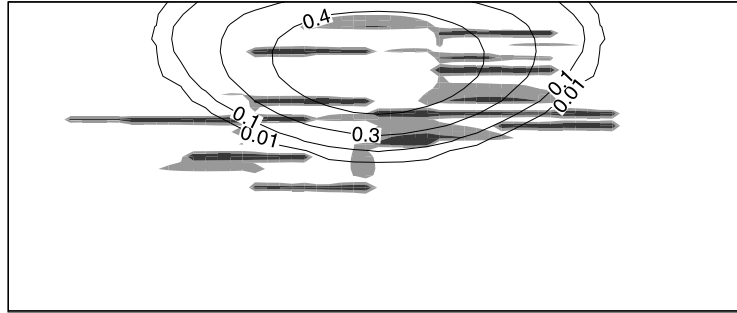


Figure 15. Comparison between numerical results with the resolved lenses (grey scales) and the upscaled parameters (contour lines).

In order to compare the results we calculated the first and second moments for the three different set-ups at three different times. Figures 16 and 17 show the saturation distributions after 20 and 40 minutes, respectively. The origin of the coordinate system is located at the midpoint of the top boundary, with the  $z$ -coordinate pointing downwards. The moments are given in Table 2. As the geometric-average and the upscaled configuration are obviously symmetric with respect to the  $z$ -axis the first moment in  $x$ -direction is not shown. The moments calculated for the geometric averaging case after 40 and 60 minutes are written in brackets, because at that time the DNAPL is already pooling at the bottom of the domain.

Table 2 shows that the results for the upscaled simulation are better than in the geometric averaging case. In the geometric averaging case the moments are significantly overestimated in the  $z$ -direction and underestimated in the  $x$ -direction. The moments for the upscaled case still underestimate all spatial moments of the discrete case. This is expected for the second moment in  $x$ -direction, where the underestimation is most pronounced, as the lenses transport DNAPL more efficiently to boundary regions than can be captured by the effective upscaled parameters.

## 6. Final Remarks

We have presented a quick and simple upscaling technique for DNAPL infiltration at the laboratory scale. We have applied the method to experimental data of a

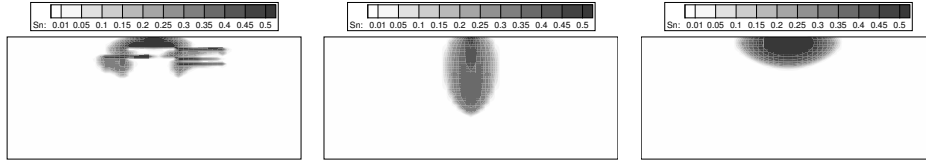


Figure 16. Saturation Distribution after 20 minutes – left: discrete simulation – middle: geometric averaging – right: upscaled parameters

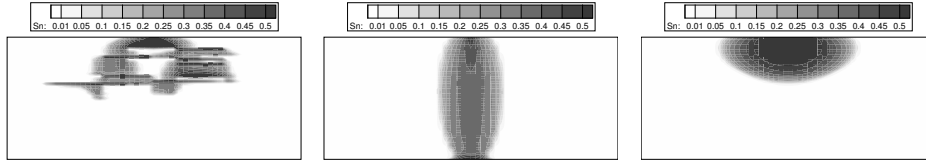


Figure 17. Saturation Distribution after 40 minutes – left: discrete simulation – middle: geometric averaging – right: upscaled parameters

sandbox experiment. The results are promising, since the overall spatial extent of the DNAPL plume could be approximated well.

Our approach consists of a percolation model to obtain the macroscopic  $P_c$ - $S$ -relationship and of a single-phase flow-approach to determine the effective permeabilities as a function of mean saturation. Currently, we use a site percolation model, which should be replaced by an invasion percolation model in the near future. The single-phase flow-model for the upscaling of relative permeability is especially useful when the system is strongly anisotropic, and the renormalization approach would fail. In the current application, both the single-phase flow-model and the renormalization approach yield strong macroscopic residual saturations and anisotropic behaviour as shown earlier by e.g. (Pickup and Sorbie, 1996).

The presented upscaling approach is subject to the following underlying assumptions:

- Capillary equilibrium is assumed.
- The fluctuations of the flow velocities and the parameter functions are neglected in the dimensional analysis.
- We have not upscaled the form of the equation but determined effective parameters assuming that the form of the equation is conserved.

The approach is therefore restricted to capillary dominated systems. Also this upscaling method is only applicable to the specific scales used in here.

Especially the capillary equilibrium assumption needs further analysis. The method should also be compared to homogenization theory (cf. e.g. (Duijn et al., 2002)). Further examinations of the influence of different heterogeneities on multi-phase flow, e.g. pooling and the influence of lenses needs investigations

Table 2. First and second moments of the DNAPL body.

time	20 min	40 min	60 min
1. moment z-direction [ $m$ ]:			
discrete	0.0650	0.1127	0.1582
geometric	0.1421	(0.2472)	(0.3388)
upscaled	0.0472	0.0724	0.0993
2. moment z-direction [ $m^2$ ]:			
discrete	0.0016	0.0039	0.0059
geometric	0.0069	(0.0195)	(0.0220)
upscaled	0.0011	0.0023	0.0035
2. moment x-direction [ $m^2$ ]:			
discrete	0.0181	0.0276	0.0381
geometric	0.0024	(0.0037)	(0.0131)
upscaled	0.0087	0.0160	0.0229

which should be accompanied by more laboratory experiments.

Up to now, only the main axis of a full  $k_r - S$  tensor is implemented in the numerical code. An extension to include the full tensor is planned in the near future.

## Acknowledgements

This work was supported by the Deutsche Forschungsgemeinschaft (DFG) in the framework of the project MUSKAT (He-2531/2-2) and the Emmy-Noether program (Ne 824/2-1, Ci 26/3-4). We are grateful to the team of the VEGAS facility for their cooperation, and to the two referees for their useful comments and suggestions.

## References

- H. Kobus, U. de Haar. *Perspektiven der Wasserforschung*, DFG, 1995.
- J. Allan, J. Ewing, J. Braun, and R. Helmig. *Scale Effects in Multiphase Flow Modeling*, In First International Conference on Remediation of Chlorinated and Recalcitrant Compounds, Non-aqueous Phase Liquids, G. B. Wickramanayake and R. E. Hinchey Monterey / California, USA, 1998.
- H. Kobus, J. Braun, and J. Allan. *Abschlussbericht 'Parameteridentifikation in Mehrphasensystemen'*. Scientif Report HG 274 WB 00/07, Institut für Wasserbau.
- H. Jakobs, R. Helmig, C. T. Miller, H. Class, M. Hilpert, and C. E. Kees. *Modelling of DNAPL flow in saturated heterogeneous porous media*, Preprint 25, Sonderforschungsbereich 404, Mehrfeldprobleme in der Kontinuumsmechanik, Universitt Stuttgart, 2003.

- T. H. Illangasekare, J. L. Ramsay, K. H. Jensen, and M. B. Butts *Experimental study of movement and distribution of dense organic contaminants in heterogeneous aquifers*, Journal of Contaminant Hydrology, 20 (1-2): 1 – 25, 1995.
- M. A. Christie, *Upscaling for Reservoir Simulation*, Journal of Petroleum Technology, 48 (11): 1004 – 1010, 1996.
- G. E. Pickup, K. S. Sorbie. *The scaleup of Two-Phase Flow in Porous Media Using Phase Permeability Tensors*, SPE Journal, December 1996.
- M. Dale, S. Ekrann, J. Mykkeltveit, and G. Virnovsky. *Effective Relative Permeabilities and Capillary Pressure for One-Dimensional Heterogeneous Media*. Transport in Porous Media, 26: 229–260, 1997.
- Y. C. Chang and K. K. Mohanty. *Scale-up of two-phase flow in heterogeneous porous media*. Journal of Petroleum Science and Engineering, 18: 21 –34, 1997.
- A. J. Desbarats. *Upscaling capillary pressure-saturation curves in heterogeneous porous media*. Water Resources Research, 31(2): 281 – 288, 1995.
- T. C. J. Yeh, L. W. Gelhar, and A. L. Gutjahr. *Stochastic Analysis of Unsaturated Flow in Heterogeneous Soils 3 . Observations and Applications*. Water Resources Research, 21(4): 465 – 471, 1985.
- A. Mantoglou and L. Q. Gelhar. *Stochastic Modelling of Large-Scale Transient Unsaturated Flow Systems*. Water Resources Research, 23(1): 37–46, 1987.
- C-M. Chang et al. *Stochastic analysis of two-phase flow in porous media: I. Spectral/perturbation approach*, Transport in Porous Media, 19, 233-259, 1995.
- I. Neuweiler, S. Attinger, W. Kinzelbach, and P. R. King. *Large Scale Mixing for Immiscible Displacement in Heterogeneous Porous Media*, Transport in Porous Media, 51: 287 – 314, 2003.
- Y. Efendiev and L. J. Durlofsky. *A Generalized Convection-Diffusion Model for Subgrid Transport in Porous Media*, submitted to SIAM MMS, 2003.
- M. Quintard and S. Whitaker. *Two-Phase Flow in Heterogeneous Porous Media: The Method of Large-Scale Averaging*. Transport in Porous Media, 3: 357–413, 1988.
- A. Ahmadi and M. Quintard. *Large-scale properties for two-phase flow in random porous media*, Journal of Hydrology, 183: 69 – 99, 1996.
- A. E. Sáez, C. J. Otero, and I. Rusinek. *The effective homogenous behaviour of heterogeneous porous media*. Transport in Porous Media, page 213–238, 1989.
- A. Bourgeat and M. Panfilov. *Effective two-phase flow through highly heterogeneous porous media: Capillary nonequilibrium effects*, Computational Geosciences, 2, 191 – 215, 1998.
- Y. S. Wu and K. Pruess. *A Multiple-Porosity Method for Simulation of Naturally Fractured Petroleum Reservoirs*. Society of Petroleum Engineers, SPE 15129, page 335–349, 1986.
- K. Pruess. *On the Validity of a Fickian Diffusion Model for the Spreading of liquid Infiltration Plumes in Partially Saturated Heterogeneous Media*. Computational Methods in Water Resources, 10: 537 – 544, 1994.
- K. Pruess. *A Fickian Diffusion Model for the Spreading of Liquid Plumes Infiltrating in Heterogeneous Media*. Transport in Porous Media, 24: 1–33, 1996.
- A. T. Corey and C. H. Rathjens. *Effect of Stratification on Relative Permeability*, Journal of Petroleum Technology, 69 – 71, 1956.
- E. H. Smith. *The Influence of Small-Scale Heterogeneity on Average Relative Permeability*, Reservoir Characterization II, 52 – 76, 1991, Academic Press, Inc.
- S. Ekrann and M. Dale and K. Langaas and J. Mykkeltveit. *Capillary Limit Effective Two-Phase Properties for 3D Media*, Society of Petroleum Engineers, SPE 35493, 119 – 129, 1996.
- Y. C. Yortsos, C. Satik, J. C. Bacri, and D. Salin. *Large-scale percolation theory of drainage*. Transport in Porous Media, 10: 171–195, 1993.
- B. H. Kueper and B. Girgrah. *Effective large-scale parameters for two-phase flow in heterogeneous porous media*. In Transport and Reactive Processes in Aquifers, page 531 – 536. Dracos & Stauffer, 1994.
- T. R. Green, J. E. Constanaz, and D. L. Freyberg. *Upscaled soil-water retention using van Genuchten's function*. Journal of Hydrologic Engineering, 1(3), 1996.

- G. E. Pickup, and K. D. Stephen. *An Assessment of steady-state scale-up for small-scale geological models*, Petroleum Geoscience, Vol. 6, 203 – 210, 2000.
- C. Braun, R. Helmig, and S. Manthey. *Determination of constitutive relationships for two-phase flow processes in heterogeneous porous media with emphasis on the relative permeability-saturation-relationship*, Journal of Contaminant Hydrology, 67(1-2): 47-85, 2003.
- C. M. Marle. *Multiphase Flow in Porous Media*, 1. edition, Institut Francais du Petrole, Paris, 1981.
- R. Helmig. *Multiphase Flow and Transport Processes in the Subsurface*, Springer-Verlag, Heidelberg, 1997.
- C.J. van Duijn, A. Mikelic, and I.S. Pop. *Effective Equations for Two-Phase Flow with Trapping on the Micro Scale*, SIAM J. Appl. Math., 62(5): 1531-1568, 2002.
- D. Stauffer. *Introduction to Percolation Theory*, Taylor & Francis, London, 1985.
- J. K. Williams. *Simple Renormalisation Schemes for Calculating Effective Properties of Heterogeneous Reservoirs*, in 1st European Conference on the Mathematics of Oil Recovery, Cambridge, UK, 1989.
- P. R. King. *Upscaling Permeability: Error Analysis for Renormalisation*. Transport in Porous Media, 23: 337–354, 1996.
- R. H. Brooks, and A. T. Corey. *Properties of porous media affecting fluid flow*, Journal of the Irrigation and Drainage Division Proceedings of the American Society of Engineers, 1966, volume 92, IR2, pages 61 - 88.
- B. B. Dykaar and P. K. Kitanidis *Determination of the Effective Hydraulic Conductivity for Heterogeneous Porous Media Using a Numerical Spectral Approach. 1. Method*, Water Resour. Res., 28 (4), pages 1155-1166 , 1992.
- L. J. Durlofsky. *Numerical Calculation of Equivalent Grid Block Permeability Tensors for Heterogenous Porous Media*, Water Resources Research, 27(5): 699 – 708, 1991.
- C. Braun *Ein Upscaling Verfahren für Mehrphasenströmungen in porösen Medien*, Forschungsbericht 103, Ph.D. Thesis, Mitteilungen des Instituts für Wasserbau, Universität Stuttgart, Stuttgart, 2000.

